analytical chemistry

pubs.acs.org/ac Article

A Dual Functional Self-Enhanced Electrochemiluminescent Nanohybrid for Label-Free MicroRNA Detection

Zhenqiang Ning, Erli Yang, Yongjun Zheng, Mengyuan Chen, Guoqiu Wu, Yuanjian Zhang, and Yanfei Shen*

Cite This: *Anal. Chem.* 2021, 93, 8971−8977 Read Online

ACCESS | Metrics & More | Article Recommendations | Supporting Information

ABSTRACT: The development of electrochemiluminescent (ECL) emitters with both intense ECL and excellent film-forming properties is highly desirable for biosensing applications. Herein, a facile one-pot preparation strategy was proposed for the synthesis of a self-enhanced ECL emitter by co-doping $Ru(bpy)_3^{2+}$ and (diethylaminomethyl)-triethoxysilane (DEAMTES) into an in situ-produced silica nanohybrid (DEAMTES@$RuSiO_2$). DEAMTES@$RuSiO_2$ not only possessed improved ECL properties but also exhibited outstanding film-forming ability, which are both critical for the construction of ECL biosensors. By coupling branched catalytic hairpin assembly with efficient signal amplification peculiarity, a label-free ECL biosensor was further constructed for the convenient and highly sensitive detection of miRNA-21. The as-fabricated ECL biosensor displayed a detection limit of 8.19 fM, much lower than those in previous reports for miRNA-21 and showed superior reliability for detecting miRNA-21-spiked human serum sample, demonstrating its potential for applications in miRNA-associated fundamental research and clinical diagnosis.

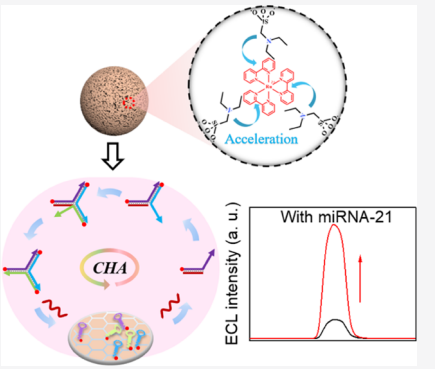

INTRODUCTION

MicroRNAs (miRNAs), a category of endogenous, non-coding, and small RNA molecules (approximately 19−23 nucleotides), are involved in various biological processes and hence closely associated with the initiation and development of different human diseases.[1−4] However, the detection of miRNA at the expression level, which is crucial for fundamental research and disease diagnosis, has been challenged by the essential characteristics of miRNAs, including a small size, sequence similarity, and low concentration.[5,6] Therefore, developing reliable and sensitive detection strategies for miRNA is desirable for both fundamental research and clinics.

Electrochemiluminescence (ECL), the electrochemical redox reaction-induced emission phenomenon of luminophores,[7−9] is an emerging powerful analytical technology with the advantages of a low background, high sensitivity, and simple operation. The generation of ECL can occur through either an annihilation mechanism or a coreactant route. For the latter, ECL is usually generated from two different precursors, e.g., luminophores and coreactants. As the most extensively studied ECL systems and standard emitters in clinics, tris(bipyridine)ruthenium(II) ($Ru(bpy)_3^{2+}$) and its derivatives demonstrate outstanding ECL properties.[10,11] Nonetheless, their ECL efficiency is limited due to the long mass and electron transfer distance between the emitter and the coreactant.[11−13] As a result, coreactant-embedded ECL emitters were proposed to overcome these obstacles by covalently attaching the coreactant to luminophores, achieving self-enhanced ECL emission without adding extra coreactants to the test solution.[14−16] To further improve the ECL efficiency, various nanomaterials such as carbon nanomaterials or metal−organic frameworks (MOFs) have been used as effective carriers for self-enhanced ECL emitters because of their large surface area and microporous structure.[17−19] However, the immobilization of self-enhanced ECL emitters on the electrode surface with sufficient stability, which relies heavily on their physicochemical characteristics, remains a challenge for biosensor construction. To this end, film-forming additives such as chitosan and Nafion are usually necessary to enhance the film stability of these nanomaterials.[20,21] It should be noted that, in electrochemical (e.g., ECL) biosensing, the participation of these additives would lead to a compromise of both mass and electron transport, which would affect the ECL efficiency significantly.[22] Thus, developing alternative ways to synthesize self-enhanced ECL emitters with excellent ECL efficiency and film-forming properties is desirable but still challenging.

Received: April 13, 2021
Accepted: June 9, 2021
Published: June 17, 2021

https://doi.org/10.1021/acs.analchem.1c01570
Anal. Chem. 2021, 93, 8971−8977

Herein, a facile one-pot strategy was proposed for the synthesis of a self-enhanced ECL emitter with an excellent film-forming property, which was realized by co-doping $Ru(bpy)_3^{2+}$ and (diethylaminomethyl)triethoxysilane (DEAMTES) into in situ-produced silica nanoparticles (DEAMTES@$RuSiO_2$) (Figure 1a). As silane, DEAMTES is

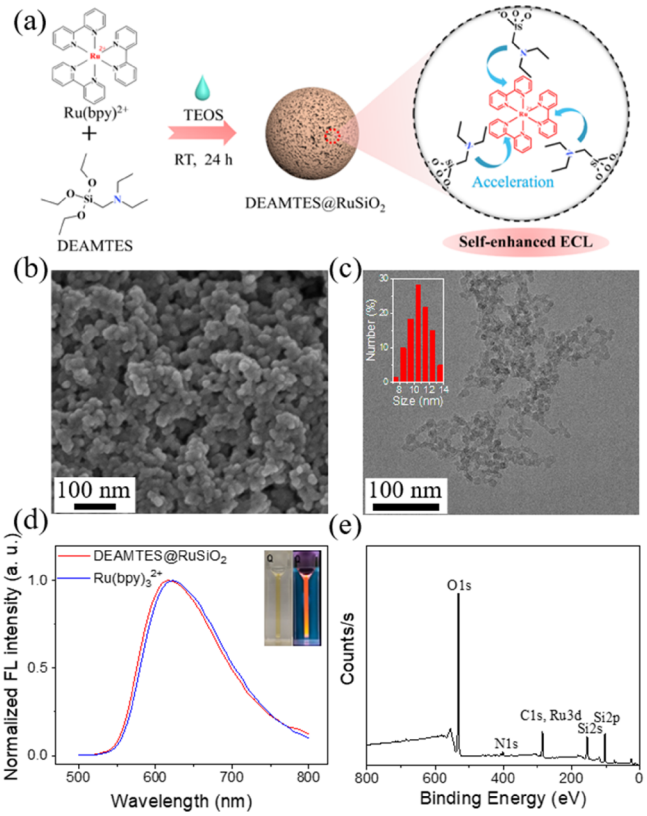

Figure 1. (a) Schematic illustration of the one-pot preparation of DEAMTES@$RuSiO_2$. (b) SEM and (c) TEM images of DEAMTES@$RuSiO_2$. The inset is the size distribution of DEAMTES@$RuSiO_2$ from the TEM results. (d) Fluorescence spectra (λ_{ex} = 450 nm) of $Ru(bpy)_3^{2+}$ solution (blue line) and DEAMTES@$RuSiO_2$ dispersion (red line). The concentrations of $Ru(bpy)_3^{2+}$ and DEAMTES@$RuSiO_2$ were 3.33 μM and 0.1 mg/mL, respectively. The inset shows a photograph of the DEAMTES@$RuSiO_2$ solution under sunlight (left) and UV light irradiation (right). (e) XPS survey spectrum of DEAMTES@$RuSiO_2$.

easily covalently incorporated into the SiO_2 matrix and is expected to be an effective coreactant. However, it has not been applied as a coreactant for $Ru(bpy)_3^{2+}$ in ECL studies. In this study, the as-synthesized DEAMTES@$RuSiO_2$ nanohybrid possessed not only remarkable self-enhanced ECL emission but also excellent film-forming properties, which are both critical for sensor performance. Furthermore, by employing catalytic hairpin assembly (CHA) as a molecular recognition unit and a signal amplification strategy,[23,24] a label-free "signal on" ECL biosensor was constructed for miRNA-21 detection. This work will envision more effective applications from eliminating additional coreactants, emitter carriers, and film-forming reagents in conventional ECL pathways.

EXPERIMENTAL SECTION

Materials and Reagents. Tris(2,2′-bipyridyl)-dichlororuthenium(II) hexahydrate ($Ru(bpy)_3Cl_2{\cdot}6H_2O$), Igepal CO-520, tetraethoxysilicon (TEOS), and tripropylamine (TPA) were purchased from Sigma-Aldrich Chemical Co. (St. Louis, MO, USA). (Diethylaminomethyl)triethoxysilane (DEAMTES) was purchased from J&K Scientific Ltd. (Beijing, China). All the DNA oligonucleotides listed in Table S1 are synthesized by Sangon Biotech Co. Ltd. (Shanghai, China).

Preparation of the DEAMTES@$RuSiO_2$ Nanohybrid. The DEAMTES and $Ru(bpy)_3^{2+}$-codoped silica nanohybrid (DEAMTES@$RuSiO_2$) was synthesized by using a ternary microemulsion system.[25,26] Typically, 1.92 g of Igepal CO-520 was dispersed in 5 mL of cyclohexane under vigorous stirring. Then, 333 μL of 10 mM $Ru(bpy)_3^{2+}$ aqueous solution and 30 μL of $NH_3{\cdot}H_2O$ (28.0-30.0%) were sequentially added to the above mixture. After continuous stirring for 30 min, 10 μL of DEAMTES was added, and the mixture was stirred for another 15 min. Finally, by adding 82 μL of TEOS, the reaction mixture was stirred for an additional 24 h. After breaking the microemulsion with acetone, the resulting nanoparticles were collected by centrifugation and washed with ethanol. The DEAMTES@$RuSiO_2$ nanohybrid was dispersed in water and stored at 4 °C in the dark before use.

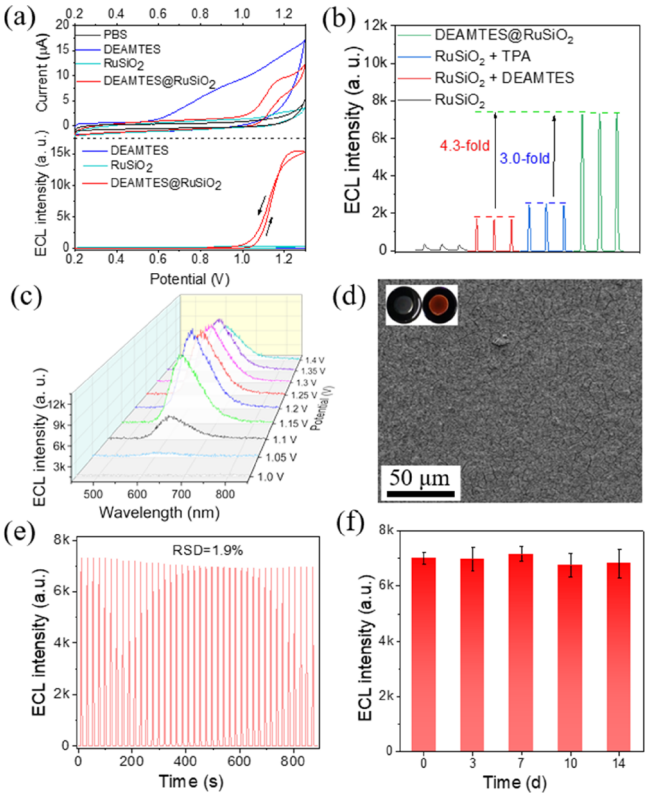

Figure 2. (a) CV and ECL-potential curves of DEAMTES, $RuSiO_2$, and DEAMTES@$RuSiO_2$ in 0.01 M PBS (pH 7.4). (b) Comparison of ECL intensities of $RuSiO_2$, $RuSiO_2$ + DEAMTES, $RuSiO_2$ + TPA, and DEAMTES@$RuSiO_2$ in 0.01 M PBS (pH 7.4). (c) ECL spectra of DEAMTES@$RuSiO_2$ in 0.01 M PBS (pH 7.4) collected at different potentials. (d) SEM image of the DEAMTES@$RuSiO_2$ film on the GCE. Inset: photographs of the DEAMTES@$RuSiO_2$/GCE with (right) and without (left) UV light irradiation. (e) ECL signals of the DEAMTES@$RuSiO_2$/GCE upon successive scanning for 900 s after the pretreatment of electrochemical oxidation in 0.01 M PBS (pH 7.4). (f) ECL signals of the DEAMTES@$RuSiO_2$/GCE in 0.01 M PBS (pH 7.4) during storage of 14 days at room temperature under darkness.

https://doi.org/10.1021/acs.analchem.1c01570
Anal. Chem. 2021, 93, 8971−8977

Feasibility of CHA Amplification Systems by PAGE Electrophoresis. For the pretreatment of hairpin probe DNA, the DNA-dissolved buffer (50 mM Na_2HPO_4, 0.5 M NaCl, pH = 6.8) was heated to 90 °C for 5 min and then slowly cooled to room temperature. The feasibility of the designed CHA amplification strategy was confirmed through PAGE electrophoretic analysis of the hairpin assembly products. Typically for lane 5 in Figure 3b, 2 μL of reaction buffer and 2 μL of 5 μM H1, H2, and H3 were thoroughly mixed by pipetting, and then 2 μL of 5 μM miRNA-21 was added and mixed. The mixture reacted at room temperature for 2 h. After that, 5 μL of the above sample was uploaded to a 10% native PAGE gel for electrophoresis analysis. Finally, the PAGE gel was imaged under UV irradiation after staining with 1% ethidium bromide (EB) solution.

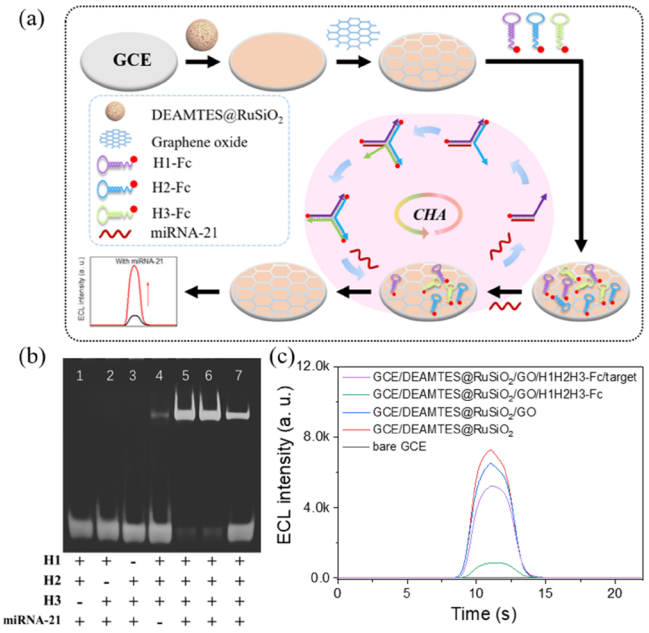

Figure 3. (a) Construction and detection procedure of the proposed ECL biosensor. (b) Feasibility analysis of the designed CHA amplification systems by PAGE electrophoresis. Lane 1: H1 + H2, lane 2: H1 + H3, lane 3: H2 + H3, lane 4: H1 + H2 + H3, lane 5: H1 + H2 + H3 + 1 μM miRNA-21, lane 6: H1 + H2 + H3 + 0.1 μM miRNA-21, and lane 7: H1 + H2 + H3 + 0.01 μM miRNA-21. The final concentrations of H1, H2, and H3 used in all these experiments were 1 μM. The concentrations of miRNA-21 used in lanes 5, 6, and 7 were 1, 0.1, and 0.01 μM, respectively. (c) ECL curves of various modified electrodes. The ECL measurements were performed in 0.01 M PBS (pH 7.4). The concentration of the target (miRNA-21) is 100 pM.

Fabrication and Sensing Procedures of the ECL Biosensor. For the preparation of the DEAMTES@$RuSiO_2$-modified electrode, the glassy carbon electrode (GCE) was polished with 0.3 μm alumina powder and successively ultrasonically cleaned with ultrapure water and ethanol and dried in air. Then, 5 μL of DEAMTES@$RuSiO_2$ solution was dropped onto the GCE surface and dried overnight. After that, the DEAMTES@$RuSiO_2$/GCE was pre-oxidized at a constant potential of 1.2 V for 40 s in 0.01 M PBS (pH 7.4) before ECL measurements.[27] It was supposed that such pre-oxidation would produce sufficient oxidized emitters and coreactants for a stabilized ECL. To prepare the ECL biosensor, 5 μL of 0.2 mg/mL graphene oxide (GO) nanosheets (prepared according to a previous report[28]) was dropped onto the DEAMTES@$RuSiO_2$/GCE and kept for 2 h at room temperature. The modified electrode was subsequently incubated with 10 μL of a mixture of H1-Fc, H2-Fc, and H3-Fc (1:1:1, 0.2 μM) for 2 h. Therefore, the as-designed ECL biosensor was fabricated. For ECL sensing, miRNA-21 samples with different concentrations were incubated with the biosensor for 2 h at room temperature. After rinsing with PBS to release the H1-Fc/H2-Fc/H3-Fc DNA trimers, ECL measurements of the biosensor were performed in 0.01 M PBS (pH 7.4) in a range from 0.2 to 1.3 V at a scan rate of 0.1 V/s.

RESULTS AND DISCUSSION

Characterization of the DEAMTES@$RuSiO_2$ Nanohybrid. The DEAMTES@$RuSiO_2$ nanohybrid was synthesized by a one-pot co-condensation strategy, in which TEOS and DEAMTES were both applied as silica sources (Figure 1a). The morphology of DEAMTES@$RuSiO_2$ was characterized by scanning electron microscopy (SEM) and transmission electron microscopy (TEM). DEAMTES@$RuSiO_2$ had a highly cross-linked quasi-spherical morphology with an average size around at 10.7 ± 1.3 nm (Figure 1b,c and the inset in Figure 1c). As shown in Figure S1a, the UV−vis spectrum of $Ru(bpy)_3^{2+}$ shows the characteristic adsorption peaks at 243, 254, 286, 422, and 454 nm. Among them, the peaks at 243 and 254 nm are attributed to the metal-centered d−d transition of $Ru(bpy)_3^{2+}$, the peak at 286 nm is assigned as the ligand-centered $\pi-\pi^*$ transition of $Ru(bpy)_3^{2+}$, and peaks at 422 and 454 nm belong to the metal-to-ligand charge transfer of $Ru(bpy)_3^{2+}$.[29,30] It should be noted that DEAMTES@$RuSiO_2$ maintained the characteristic absorption from $Ru(bpy)_3^{2+}$, verifying the successful doping of $Ru(bpy)_3^{2+}$ into the in situ-produced silica matrix. On the other hand, the DEAMTES@$RuSiO_2$ nanohybrid showed excellent dispersibility in an aqueous solution and orange emission under UV light irradiation (inset in Figure 1d). As shown in Figure 1d, the fluorescence spectrum of DEAMTES@$RuSiO_2$ exhibited a maximum emission at 617 nm, which was consistent with that of $Ru(bpy)_3^{2+}$. It should be noted that the slight blue shift of the emission could be caused by the electrostatic interaction of $Ru(bpy)_3^{2+}$ and SiO^- groups in the silica matrix.[31−33] Moreover, the fluorescence signal of DEAMTES@$RuSiO_2$ was almost maintained after storage for 7 months (Figure S1b), indicative of sufficient stability of the nanohybrid for subsequent biosensing studies.

Furthermore, the co-dopping of $Ru(bpy)_3^{2+}$ and DEAMTES in the SiO_2 matrix was verified by Fourier transform infrared spectroscopy (FTIR) and X-ray photoelectron spectroscopy (XPS). As shown in Figure S2a, the characteristic peaks from the FTIR spectrum at 1073 cm^{-1} could be assigned to the asymmetric stretching vibration of the Si−O−Si bond. In addition, the intensity of the shoulder band at 962 cm^{-1} of the Si−OH bond was depressed after the formation of DEAMTES@$RuSiO_2$, which may be caused by the interaction between $Ru(bpy)_3^{2+}$ and SiO^- groups.[34] Furthermore, the characteristic peaks of DEAMTES at 1392 cm^{-1} and $Ru(bpy)_3^{2+}$ at 664 cm^{-1} were observed in the FTIR spectrum of DEAMTES@$RuSiO_2$, verifying the co-existence of DEAMTES and $Ru(bpy)_3^{2+}$ in this nanohybrid. Meanwhile, the XPS survey spectrum of DEAMTES@$RuSiO_2$ in Figure 1e shows the characteristic peaks of O1s, Si2s, Si2p, C1s, N1s, and Ru3d, manifesting the successful synthesis of DEAMTES@$RuSiO_2$. The deconvoluted Ru3d spectrum in Figure S2b

https://doi.org/10.1021/acs.analchem.1c01570
Anal. Chem. 2021, 93, 8971−8977

shows two peaks with binding energies at 280.98 and 284.28 eV, which could be ascribed to the signals of $Ru3d_{5/2}$ and $Ru3d_{3/2}$, respectively,[35] indicative of the presence of $Ru(bpy)_3^{2+}$ in the nanohybrid. Additionally, the N1s spectrum was split into two peaks at 402.08 and 400.08 eV (Figure S2c), corresponding to the C═N bond of the pyridine ring and the C−N bond of tertiary amine (DEAMTES), respectively.[36] All these results demonstrated the successful preparation of DEAMTES@$RuSiO_2$.

ECL Performance of DEAMTES@$RuSiO_2$. As silane, DEAMTES could be easily covalently incorporated into the SiO_2 matrix compared to others (Figure S3) and is expected to be an effective coreactant due to the presence of the tertiary amine group. However, it has not been applied as a coreactant for $Ru(bpy)_3^{2+}$ on the ECL studies. As shown in Figure 2a, only a weak ECL signal was observed from $RuSiO_2$ in PBS solution. After the addition of DEAMTES@$RuSiO_2$ to the solution, the ECL response increased, demonstrating the coreactant effect of DEAMTES on $Ru(bpy)_3^{2+}$ in the ECL process. Surprisingly, DEAMTES@$RuSiO_2$ exhibited a much stronger ECL emission without adding any extra coreactant. To improve the ECL performance, the molar ratios of DEAMTES:TEOS and DEAMTES:$Ru(bpy)_3^{2+}$ were optimized during the preparation of the DEAMTES@$RuSiO_2$ nanohybrid. Generally, increasing the molar ratio of DEAMTES to TEOS can enhance the ECL signal by introducing more DEAMTES, but it would lead to a decreased pore volume of the SiO_2 matrix, which in turn induced a decrease in the ECL signal due to the insufficient $Ru(bpy)_3^{2+}$ loading. As shown in Figure S4a, increasing the ratio from 0.05 to 0.1 led to an increase in the ECL intensity, and further increasing the ratio resulted in a decrease in the ECL signal. In addition, the molar ratio of DEAMTES and $Ru(bpy)_3^{2+}$ also plays a vital role for the ECL signal generation. As shown in Figure S4b, the highest ECL intensity of DEAMTES@$RuSiO_2$ was obtained at a ratio of DEAMTES:$Ru(bpy)_3^{2+}$ at 11:1. It is supposed that the maximum ECL intensity could be achieved when DEAMTES and $Ru(bpy)_3^{2+}$ are doped in the proper proportion. Therefore, the molar ratios of DEAMTES:TEOS and DEAMTES:$Ru(bpy)_3^{2+}$ were optimized at 1:10 and 11:1, respectively. As shown in Figure 2b, under these optimum conditions, DEAMTES@$RuSiO_2$ shows a 4.3-fold higher ECL response than $Ru(bpy)_3^{2+}$/DEAMTES and a 3-fold higher response than the traditional $Ru(bpy)_3^{2+}$/TPA system. The much more intense ECL response could be attributed to the short mass, electron transfer distance, and low energy loss. To gain insight into the ECL mechanism, CV and ECL-potential curves of individual DEAMTES and $RuSiO_2$ in PBS were recorded. As shown in Figure 2a, DEAMTES and $RuSiO_2$ displayed onset oxidization potentials at approximately 0.58 and 1.04 V, respectively, which suggested that DEAMTES could be more easily oxidized than $RuSiO_2$. It is worth noting that the ECL emission of DEAMTES@$RuSiO_2$ was observed with an onset potential at 1.03 V, which was highly consistent with the onset potential of $RuSiO_2$ oxidation. In addition, the ECL spectra of DEAMTES@$RuSiO_2$ collected at different potentials displayed that the onset potential was at around 1.05 V with a peak wavelength at approximately 610 nm, assigning to the emission of $RuSiO_2$ (Figure 2c), indicating that the ECL signal was generated after the oxidation of both DEAMTES and $Ru(bpy)_3^{2+}$. Thus, the ECL reaction of DEAMTES@$RuSiO_2$ was driven by an "oxidation−reduction" coreactant route.[8,37] Based on above results, the possible ECL reaction mechanism for DEAMTES@$RuSiO_2$ is deduced in Scheme S1. Briefly, during the anodic scanning, DEAMTES was first electrochemically oxidized to $DEAMTES^{\cdot+}$ at 0.58 V. Meanwhile, the deprotonation reaction of $DEAMTES^{\cdot+}$ was initiated, producing the reductive $DEAMTES^{\cdot}$ radical. Afterward, $Ru(bpy)_3^{2+}$ was electrochemically oxidized to $Ru(bpy)_3^{3+}$ on the electrode surface at 1.04 V, which was then reduced by $DEAMTES^{\cdot}$ to form the excited state $Ru(bpy)_3^{2+*}$ intermediate. Finally, $Ru(bpy)_3^{2+*}$ returned to the ground state and emitted light.[7]

It is worth noting that DEAMTES@$RuSiO_2$ displayed not only enhanced ECL emission but also excellent film-forming ability. It is well known that the immobilization of nanomaterials on the surface of substrates as a form of a robust film is essential for their biosensing applications.[38−40] For this purpose, additives such as chitosan and Nafion are usually used as binders to enhance the adhesion of nanomaterials on the substrate to enhance the film quality. However, for electrochemical (e.g., ECL) biosensing, the participation of these additives would lead to a compromise of both mass and electron transport, which would affect the ECL efficiency significantly.[22,41] In this work, DEAMTES@$RuSiO_2$ could form a robust film on the electrode surface (Figure 2d) without any film-forming additives, thus enabling stable ECL reactions under continuous scanning without detachment. As shown in Figure 2e, after pretreatment of electrochemical oxidation, the DEAMTES@$RuSiO_2$/GCE exhibited a stable ECL signal with a relative standard deviation (RSD) of 1.9% upon a continuous scan for 900 s in PBS.[27] Moreover, a 97.1% initial signal of the DEAMTES@$RuSiO_2$/GCE was maintained after 2 weeks of storage (Figure 2f). To get more insights for the excellent film-forming ability of DEAMTES@$RuSiO_2$ on the GCE surface, the $RuSiO_2$/GCE and $Ru(bpy)_3^{2+}$/GCE were investigated as controls, and their film stability was evaluated. All these modified GCEs after drying overnight were washed with H_2O, and the integrity of these films was observed under the irradiation of UV light (Table S2). As shown in Table S2, the $RuSiO_2$ film on the GCE was partly retained after washing, while the whole film of $Ru(bpy)_3^{2+}$ was almost detached from the GCE surface, indicating that the $RuSiO_2$ film was more stable than the $Ru(bpy)_3^{2+}$ film. Therefore, the participation of SiO_2 was in favor of enhancing the film stability, presumably due to the physical adsorption of SiO_2 on the electrode surface. More interestingly, the DEAMTES@$RuSiO_2$ film was almost intact after the same treatment, implying the critical role of DEAMTES in stabilizing the film on the electrode surface, which could be ascribed to the hydrogen-bonding interaction between the tertiary amine groups on DEAMTES and the hydroxyl groups on the GCE surface.[42] Thus, both the physical adsorption of SiO_2 on the electrode surface and the hydrogen-bonding interaction between DEAMTES and the electrode played crucial roles in enhancing the film-forming ability. It should be noted that both the self-enhanced ECL and the excellent film-forming ability are highly desirable for further biosensor construction.

Construction and Characterization of the ECL Biosensor. By taking miRNA-21 as a model analyte, a label-free ECL biosensor was constructed by using DEAMTES@$RuSiO_2$ as a self-enhanced emitter (Figure 3a). Since CHA, an excellent signal amplification technique, could remarkably improve the analytical performance of ECL biosensors,[23] in the present work, a CHA signal amplification strategy was introduced to the ECL biosensor. The feasibility of the CHA

https://doi.org/10.1021/acs.analchem.1c01570
Anal. Chem. 2021, 93, 8971−8977

amplification strategy was verified via PAGE electrophoresis. As shown in Figure 3b, only one diffuse band was observed in the mixtures of any two hairpin DNA probes from H1, H2, and H3 (lanes 1, 2, and 3), indicating that they cannot interact with each other. A new weak band was observed in the mixture of three hairpin DNA probes of H1, H2, and H3 (lane 4), indicative of spontaneous hairpin assembly with an extremely low yield in the absence of miRNA-21. In contrast, in the presence of miRNA-21, the band of the assembled hairpin trimer was remarkably enhanced and the band of hairpin probe DNA almost disappeared, indicating that the CHA reaction was dramatically accelerated by miRNA-21 and that all hairpin DNA probes were consumed entirely for the assembly (lane 5). Therefore, the designed CHA strategy can specifically recognize miRNA-21. To confirm the amplification capacity of this CHA system, miRNA-21 at different concentrations was applied as an initiator for the CHA reaction. As shown in Figure 3b (lanes 6 and 7), in the presence of 0.1 and 0.01 μM miRNA-21, the yields for the hairpin assemblies of H1, H2, and H3 were 101.8 and 58.5% (compared to lane 5; estimated by ImageJ software), respectively. Therefore, considering that every CHA assembled product contains three copies of ECL signal-related Fc, the amplification factor of the as-designed CHA strategy is approximately 175.5-fold for the ECL signal, which is considerably effective for improving the sensing performance of biosensors.

The fabrication procedure of the proposed ECL biosensor is shown in Figure 3a. The hairpin DNA probes H1-Fc, H2-Fc, and H3-Fc could spontaneously absorb onto the two-dimensional planar structure of GO (TEM characterization of GO is shown in Figure S5a) on the modified GCE via $\pi-\pi$-stacking interactions,[43] resulting in quenching of the ECL signal of DEAMTES@$RuSiO_2$ due to the shortened distance of ferrocene on DNA probes and emitters. In the presence of miRNA-21, CHA reactions were initiated, eventually generating the Y-shaped hairpin trimer. The double-stranded H1-Fc/H2-Fc/H3-Fc trimer was removed from the modified GCE by washing due to the poor interaction between double-stranded DNA and GO,[43−45] which caused a significant recovery of the ECL emission of DEAMTES@$RuSiO_2$. Thus, the increased ECL signal could be used for sensitive detection of miRNA-21.

For the characterization of stepwise fabrications of the proposed biosensor, the electrochemical impedance spectroscopy (EIS) and ECL curves of various modified electrodes were recorded. As shown in Figure S5b and Table S3, the charge transfer resistance (R_{ct}) increased gradually when DEAMTES@$RuSiO_2$ and GO were coated onto the GCE, implying poor conductivity of DEAMTES@$RuSiO_2$ and GO. After the modification of H1-Fc, H2-Fc, and H3-Fc, R_{ct} further increased due to the electronic repulsion between $[Fe(CN)_6]^{3-}$ and the negatively charged DNA probe. When miRNA-21 was introduced, the probe DNA was released from the electrode surface caused by the CHA reaction, leading to an obvious decrease in R_{ct}. The above EIS results confirmed the successful fabrication of the proposed ECL biosensor.

Furthermore, the ECL response of various modified electrodes was also recorded to monitor the stepwise fabrication process of the biosensor. As shown in Figure 3c, the ECL response of the bare GCE was not detected and increased significantly after modification with DEAMTES@$RuSiO_2$, indicating its excellent ECL property. After the modification of GO, the ECL intensity was slightly decreased. The ECL intensity was dramatically reduced after the DNA probes H1-Fc, H2-Fc, and H3-Fc were introduced because the ferrocene-capped probe DNA could quench the ECL of DEAMTES@$RuSiO_2$ by hindering the charge transfer between the emitter and coreactant. Excitingly, after incubation with miRNA-21, the ECL signal was recovered because the triploid probe DNA leaves from the surface of the modified electrode, which further demonstrated that the biosensor was successfully fabricated and could be used for quantitative miRNA-21 sensing.

Analytical Performance of the ECL Biosensor. Under the optimum conditions (Figure S6), the analytical performance of the proposed biosensor was assessed by monitoring the ECL response with different concentrations of miRNA-21. As shown in Figure 4a, a gradual increase in the ECL signal was

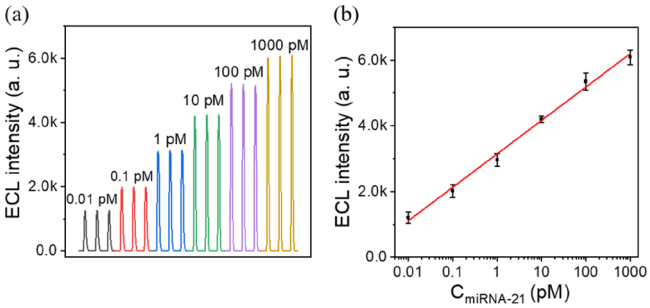

Figure 4. (a) ECL response of the biosensor toward different concentrations of miRNA-21 from 0.01 to 1000 pM. (b) Corresponding calibration curve of ECL intensity against the miRNA-21 concentration.

observed with the increase in the miRNA-21 concentration. Figure 4b shows an excellent linear relationship between the ECL intensity (I) and the logarithm of miRNA-21 concentration (lg $C_{miRNA-21}$), where the linear equation can be expressed as I = 1016.53lg $C_{miRNA-21}$ + 3147.81 (R^2 = 0.994). The proposed ECL biosensor shows a wide linear range of 0.01−1000 pM with a limit of detection (LOD) of 8.19 fM (details of LOD calculation are shown in the Supporting Information). Moreover, the analytical performance of the established biosensor was superior to those in previous reports (Table 1), highlighting its advantages for miRNA-21 detection.

Table 1. Comparison of the Sensing Performance of Available Biosensors for miRNA-21 Detection

method	linear range (pM)	detection limit (pM)	ref
fluorescence	50 −1 × 10^4	1	46
fluorescence	0.1 −1 × 10^4	0.032	47
electrochemistry	1 −1 × 10^5	1	48
electrochemistry	0.1−1000	0.03	49
photoelectrochemistry	0.1 −1 × 10^4	36	50
ECL	1 −1 × 10^6	0.12	51
ECL	0.01−1000	8.19 × 10^{-3}	this work

To assess the specificity, the ECL response of the proposed biosensor against several common interfering miRNAs, including miRNA-16, miRNA-141, and miRNA-155, was recorded. As shown in Figure 5a, compared with those of miRNA-21 and the mixture, the ECL response of the biosensor to the interfering miRNAs was much lower, indicating

https://doi.org/10.1021/acs.analchem.1c01570
Anal. Chem. 2021, 93, 8971−8977

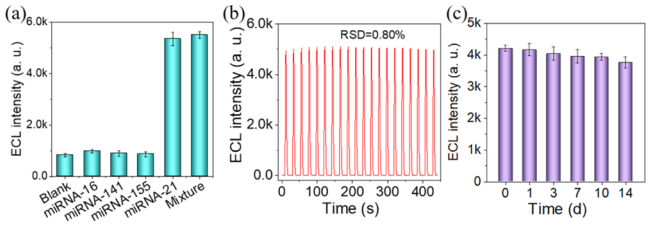

Figure 5. (a) Selectivity of the proposed biosensor toward various miRNAs with a concentration of 100 pM. (b) Signal stability of the proposed biosensor incubated with 100 pM miRNA-21 under consecutive scans for 20 cycles. (c) Storage stability of the biosensor. The ECL testing was performed in 0.01 M PBS (pH 7.4).

excellent selectivity of this biosensor. In addition, the proposed biosensor showed a stable ECL signal with an RSD of 0.80% upon successive scanning for 20 cycles (Figure 5b). To further evaluate the stability, the biosensor was stored at 4 °C in the dark. As shown in Figure 5c, 89.4% of the initial ECL signal was retained after storage for 14 days, demonstrating satisfactory stability of the proposed biosensor.

Preliminary Analysis of miRNA-21 in Real Samples. The practical feasibility and reliability of the proposed sensing systems were estimated via a recovery experiment by spiking different amounts of miRNA into 1% diluted human serum. Five spiked samples with different concentrations of miRNA-21 (0.01, 1, and 1000 pM) were measured, and the concentrations were calculated, according to the calibration curve in Figure 4b. As shown in Table S4, the recoveries of miRNA-21 ranged from 93.2 to 108.31%, with an RSD less than 9.06%, exhibiting the high reliability of the established biosensor for practical sensing of miRNA-21.

CONCLUSIONS

In summary, we developed a facile and convenient strategy for the one-pot preparation of a DEAMTES@RuSiO$_2$ nanohybrid with both enhanced ECL and film-forming properties by encapsulating the coreactant DEAMTES and emitter Ru(bpy)$_3^{2+}$ into in situ-produced SiO$_2$. DEAMTES@RuSiO$_2$ showed a 4.3- and 3-fold higher ECL efficiency than the traditional ECL systems of Ru(bpy)$_3^{2+}$/TPA and Ru(bpy)$_3^{2+}$/DEAMTES, respectively. Moreover, by coupling the CHA signal amplification technique, a sensitive and selective label-free ECL biosensor for detecting miRNA-21 was constructed. The proposed ECL biosensor exhibited promising sensing performance for spiked serum samples. This work would provide a new avenue for preparing self-enhanced ECL emitters and designing sensing systems for miRNA detection in biosensing and clinical fields.

ASSOCIATED CONTENT

Supporting Information

The Supporting Information is available free of charge at https://pubs.acs.org/doi/10.1021/acs.analchem.1c01570.

Apparatus, LOD calculation, proposed ECL mechanism, optimization of DEAMTES@RuSiO$_2$ preparation, UV−vis, FTIR, XPS, and ECL characterizations of DEAMTES@RuSiO$_2$, optimization of sensing conditions, sequences of the DNA/RNA oligonucleotide, EIS date of the modified electrode, and recovery experiment (PDF)

AUTHOR INFORMATION

Corresponding Author

Yanfei Shen − *Medical School, School of Chemistry and Chemical Engineering, Center of Clinical Laboratory Medicine, Zhongda Hospital, and Jiangsu Provincial Key Laboratory of Critical Care Medicine, Southeast University, Nanjing 210009, China;* orcid.org/0000-0003-0369-5920; Email: Yanfei.Shen@seu.edu.cn

Authors

Zhenqiang Ning − *Medical School, School of Chemistry and Chemical Engineering, Southeast University, Nanjing 210009, China*

Erli Yang − *Medical School, School of Chemistry and Chemical Engineering, Southeast University, Nanjing 210009, China*

Yongjun Zheng − *Medical School, School of Chemistry and Chemical Engineering, Southeast University, Nanjing 210009, China*

Mengyuan Chen − *Medical School, School of Chemistry and Chemical Engineering, Southeast University, Nanjing 210009, China*

Guoqiu Wu − *Medical School, School of Chemistry and Chemical Engineering, Center of Clinical Laboratory Medicine, Zhongda Hospital, and Jiangsu Provincial Key Laboratory of Critical Care Medicine, Southeast University, Nanjing 210009, China*

Yuanjian Zhang − *Medical School, School of Chemistry and Chemical Engineering, Southeast University, Nanjing 210009, China;* orcid.org/0000-0003-2932-4159

Complete contact information is available at: https://pubs.acs.org/10.1021/acs.analchem.1c01570

Notes

The authors declare no competing financial interest.

ACKNOWLEDGMENTS

This work is supported by the National Natural Science Foundation of China (22074015 and 21775018) and the Postgraduate Research & Practice Innovation Program of Jiangsu Province (KYCX19_0119).

REFERENCES

(1) Bartel, D. P. *Cell* **2004**, *116*, 281−297.
(2) Cheng, Y.; Dong, L.; Zhang, J.; Zhao, Y.; Li, Z. *Analyst* **2018**, *143*, 1758−1774.
(3) Dong, H.; Lei, J.; Ding, L.; Wen, Y.; Ju, H.; Zhang, X. *Chem. Rev.* **2013**, *113*, 6207−6233.
(4) Ryan, B. M.; Robles, A. I.; Harris, C. C. *Nat. Rev. Cancer* **2010**, *10*, 389−402.
(5) Peng, H.; Newbigging, A. M.; Reid, M. S.; Uppal, J. S.; Xu, J.; Zhang, H.; Le, X. C. *Anal. Chem.* **2020**, *92*, 292−308.
(6) Shin, S.; Jung, Y.; Uhm, H.; Song, M.; Son, S.; Goo, J.; Jeong, C.; Song, J.-J.; Kim, V. N.; Hohng, S. *Nat. Commun.* **2020**, *11*, 6033.
(7) Richter, M. M. *Chem. Rev.* **2004**, *104*, 3003−3036.
(8) Miao, W. *Chem. Rev.* **2008**, *108*, 2506−2553.
(9) Wu, P.; Hou, X.; Xu, J.-J.; Chen, H.-Y. *Chem. Rev.* **2014**, *114*, 11027−11059.
(10) Pan, D.; Fang, Z.; Yang, E.; Ning, Z.; Zhou, Q.; Chen, K.; Zheng, Y.; Zhang, Y.; Shen, Y. *Angew. Chem., Int. Ed.* **2020**, *59*, 16747−16754.
(11) Wang, N.; Gao, H.; Li, Y.; Li, G.; Chen, W.; Jin, Z.; Lei, J.; Wei, Q.; Ju, H. *Angew. Chem., Int. Ed.* **2021**, *60*, 197−201.
(12) Ye, J.; Liu, G.; Yan, M.; Zhu, Q.; Zhu, L.; Huang, J.; Yang, X. *Anal. Chem.* **2019**, *91*, 13237−13243.

(13) Valenti, G.; Scarabino, S.; Goudeau, B.; Lesch, A.; Jović, M.; Villani, E.; Sentic, M.; Rapino, S.; Arbault, S.; Paolucci, F.; Sojic, N. *J. Am. Chem. Soc.* **2017**, *139*, 16830−16837.
(14) Sun, S.; Yang, Y.; Liu, F.; Fan, J.; Peng, X.; Kehr, J.; Sun, L. *Dalton Trans.* **2009**, 7969−7974.
(15) Carrara, S.; Arcudi, F.; Prato, M.; De Cola, L. *Angew. Chem., Int. Ed.* **2017**, *129*, 4835−4839.
(16) Wang, T.; Wang, D.; Padelford, J. W.; Jiang, J.; Wang, G. *J. Am. Chem. Soc.* **2016**, *138*, 6380−6383.
(17) Fu, X.; Tan, X.; Yuan, R.; Chen, S. *Biosens. Bioelectron.* **2017**, *90*, 61−68.
(18) Wang, C.; Zhang, N.; Wei, D.; Feng, R.; Fan, D.; Hu, L.; Wei, Q.; Ju, H. *Biosens. Bioelectron.* **2019**, *142*, 111521.
(19) Xiong, C.; Liang, W.; Zheng, Y.; Zhuo, Y.; Chai, Y.; Yuan, R. *Anal. Chem.* **2017**, *89*, 3222−3227.
(20) Han, Z.; Shu, J.; Jiang, Q.; Cui, H. *Anal. Chem.* **2018**, *90*, 6064−6070.
(21) Yuan, Y.; Li, X.; Chen, A. Y.; Wang, H. J.; Chai, Y. Q.; Yuan, R. *Biosens. Bioelectron.* **2019**, *132*, 62−67.
(22) Liu, G.; Ma, C.; Jin, B.-K.; Chen, Z.; Zhu, J.-J. *Anal. Chem.* **2018**, *90*, 4801−4806.
(23) Ning, Z.; Zheng, Y.; Pan, D.; Zhang, Y.; Shen, Y. *Biosens. Bioelectron.* **2020**, *150*, 111945.
(24) Lu, H.-J.; Pan, J.-B.; Wang, Y.-Z.; Ji, S.-Y.; Zhao, W.; Luo, X.-L.; Xu, J.-J.; Chen, H.-Y. *Anal. Chem.* **2018**, *90*, 10434−10441.
(25) Zanarini, S.; Rampazzo, E.; Ciana, L. D.; Marcaccio, M.; Marzocchi, E.; Montalti, M.; Paolucci, F.; Prodi, L. *J. Am. Chem. Soc.* **2009**, *131*, 2260−2267.
(26) Cushing, B. L.; Kolesnichenko, V. L.; O'Connor, C. J. *Chem. Rev.* **2004**, *104*, 3893−3946.
(27) Peng, H.; Huang, Z.; Sheng, Y.; Zhang, X.; Deng, H.; Chen, W.; Liu, J. *Angew. Chem., Int. Edit.* **2019**, *58*, 11691−11694.
(28) Zhang, Y.; Fugane, K.; Mori, T.; Niu, L.; Ye, J. *J. Mater. Chem. B* **2012**, *22*, 6575−6580.
(29) Kalyanasundaram, K. *Coord. Chem. Rev.* **1982**, *46*, 159−244.
(30) Bertoncello, P.; Dennany, L.; Forster, R. J.; Unwin, P. R. *Anal. Chem.* **2007**, *79*, 7549−7553.
(31) Qian, L.; Yang, X. R. *Adv. Funct. Mater.* **2007**, *17*, 1353−1358.
(32) Dang, J.; Guo, Z.; Zheng, X. *Anal. Chem.* **2014**, *86*, 8943−8950.
(33) Mirenda, M.; Levi, V.; Bossi, M. L.; Bruno, L.; Bordoni, A. V.; Regazzoni, A. E.; Wolosiuk, A. *J. Colloid Interface Sci.* **2013**, *392*, 96−101.
(34) Ahkam, Q. M.; Khan, E. U.; Iqbal, J.; Murtaza, A.; Khan, M. T. *Phys. B* **2019**, *572*, 161−167.
(35) Hong, D.; Jo, E.-J.; Kim, K.; Song, M.-B.; Kim, M.-G. *Small* **2020**, *16*, 2004535.
(36) Yang, J.-P.; Hu, H.-P.; Cheng, Z.-Y.; Qiu, X.-J.; Wang, C.-X. *Polyhedron* **2017**, *128*, 76−84.
(37) Miao, W.; Choi, J.-P.; Bard, A. J. *J. Am. Chem. Soc.* **2002**, *124*, 14478−14485.
(38) Chen, L.; Zeng, X.; Si, P.; Chen, Y.; Chi, Y.; Kim, D.-H.; Chen, G. *Anal. Chem.* **2014**, *86*, 4188−4195.
(39) Zhang, P.; Zhuo, Y.; Chang, Y.; Yuan, R.; Chai, Y. *Anal. Chem.* **2015**, *87*, 10385−10391.
(40) Wang, X.; Shang, L.; Zhang, W.; Jia, L.-P.; Ma, R.-N.; Jia, W.-L.; Wang, H.-S. *Biosens. Bioelectron.* **2019**, *141*, 111436.
(41) Zhang, H.; Han, Z.; Wang, X.; Li, F.; Cui, H.; Yang, D.; Bian, Z. *ACS Appl. Mater. Interfaces* **2015**, *7*, 7599−7604.
(42) Lv, W.; Yang, Q.; Li, Q.; Li, H.; Li, F. *Anal. Chem.* **2020**, *92*, 11747−11754.
(43) Chen, W.; Zhang, X.; Li, J.; Chen, L.; Wang, N.; Yu, S.; Li, G.; Xiong, L.; Ju, H. *Anal. Chem.* **2020**, *92*, 2714−2721.
(44) Yun, W.; Xiong, W.; Wu, H.; Fu, M.; Huang, Y.; Liu, X.; Yang, L. *Sens. Actuators B-Chem.* **2017**, *249*, 493−498.
(45) Li, F.; Huang, Y.; Yang, Q.; Zhong, Z.; Li, D.; Wang, L.; Song, S.; Fan, C. *Nanoscale* **2010**, *2*, 1021−1026.
(46) Wang, Z.; Xue, Z.; Hao, X.; Miao, C.; Zhang, J.; Zheng, Y.; Zheng, Z.; Lin, X.; Weng, S. *Anal. Chim. Acta* **2020**, *1103*, 212−219.
(47) Yang, W.; Shen, Y.; Zhang, D.; Li, C.; Yuan, R.; Xu, W. *Anal. Chem.* **2019**, *91*, 7782−7789.
(48) Shin Low, S.; Pan, Y.; Ji, D.; Li, Y.; Lu, Y.; He, Y.; Chen, Q.; Liu, Q. *Sens. Actuators B-Chem.* **2020**, *308*, 127718.
(49) Wang, D.; Chai, Y.; Yuan, Y.; Yuan, R. *Anal. Chem.* **2020**, *92*, 14197−14202.
(50) Sun, J.; Li, L.; Ge, S.; Zhao, P.; Zhu, P.; Wang, M.; Yu, J. *ACS Appl. Mater. Interfaces* **2021**, *13*, 3645−3652.
(51) Liu, G.; Hong, J.; Ma, K.; Wan, Y.; Zhang, X.; Huang, Y.; Kang, K.; Yang, M.; Chen, J.; Deng, S. *Biosens. Bioelectron.* **2020**, *150*, 111963.

https://doi.org/10.1021/acs.analchem.1c01570
Anal. Chem. 2021, 93, 8971−8977